Nonlin. Processes Geophys. Discuss., doi:10.5194/npg-2015-78, 2016
Manuscript under review for journal Nonlin. Processes Geophys.
Published: 19 January 2016

Nonlinear Processes in Geophysics
Discussions
Open Access
EGU

Subvisible cirrus clouds – a dynamical system approach

E. J. Spreitzer[1], M. P. Marschalik[1], and P. Spichtinger[1]

[1]Institute for Atmospheric Physics, Johannes Gutenberg University Mainz, Germany

Correspondence to: Peter Spichtinger (spichtin@uni-mainz.de)

Abstract. Ice clouds, so-called cirrus clouds, occur very frequently in the tropopause region. A special class are subvisible cirrus clouds with an optical depth lower than 0.03. Obviously, the ice crystal number concentration of these clouds is very low. The dominant pathway for these clouds is not known well. It is often assumed that heterogeneous nucleation at solid aerosol particles is the preferred mechanism although homogeneous freezing of aqueous solution droplets might be possible. For investigating subvisible cirrus clouds as formed by homogeneous freezing we develop a simple analytical cloud model from first principles; the model consists of a three dimensional set of ordinary differential equations, including the relevant processes as ice nucleation, diffusional growth and sedimentation, respectively. The model is integrated numerically and is investigated using theory of dynamical systems. We found two different states for the long-term behaviour of subvisible cirrus clouds, i.e. an attractor case and a limit cycle scenario. The transition between the states constitutes a Hopf bifurcation and is determined by environmental conditions as vertical updraughts and temperature. In both cases, the microphysical properties of the simulated clouds agree reasonably well with simulations using a complex model, with former analytical studies and with observations of subvisible cirrus. In addition, the model can also be used for explaining complex model simulations close to the bifurcation qualitatively. Finally, the results indicate that homogeneous nucleation might be a possible formation pathway for subvisible cirrus clouds.

1 Introduction

Clouds consisting exclusively of ice crystals, so-called cirrus clouds, are frequently found in the tropopause region in the extratropics. Satellite observations show frequencies of occurrence up to 40% in the extratropical storm tracks and upto 60% in regions of tropical convection (Stubenrauch et al., 2010). Cirrus clouds influence the energy budget of the Earth-Atmosphere system like other clouds by reflecting and scattering incoming solar radiation (albedo effect) and by absorbing and re-emitting thermal radiation (greenhouse effect). In contrast to liquid clouds the net effect of cirrus clouds on the total energy budget is not known yet, although usually a positive net effect is assumed (Chen et al., 2000). Since the formation of ice crystals requires high supersaturation (e.g.,

Nonlin. Processes Geophys. Discuss., doi:10.5194/npg-2015-78, 2016
Manuscript under review for journal Nonlin. Processes Geophys.
Published: 19 January 2016

Nonlinear Processes in Geophysics
Discussions
Open Access
EGU

Koop et al., 2000; Hoose and Möhler, 2012) and diffusional growth of ice crystals is quite slow in the low temperature regime ($T < 235\,\mathrm{K}$) cirrus clouds usually are far away from thermodynamic equilibrium. Thus, in contrast to liquid clouds, which usually coincide with their (super-)saturated environment, there can be a continuous transition from clear air over very low ice crystal number concentrations to thick cirrus clouds with high mass and number concentrations. A special class of cirrus clouds constitute the so-called subvisible cirrus clouds (SVCs), which are usually defined by an optical thickness $\tau < 0.03$ (Sassen and Dodd, 1989). These clouds are difficult to detect; usually remote sensing techniques as LIDAR or occultation observations (e.g., Wang et al., 1996) are used to detect these very thin cirrus clouds. Only few in situ measurements of subvisible cirrus clouds are available, suggesting very low values in ice crystal number concentrations (e.g., Froyd et al., 2010; Kübbeler et al., 2011). Global observations from satellites (Wang et al., 1996; Stubenrauch et al., 2010; Hoareau et al., 2013) as well as observations with stationary LIDAR systems (e.g., Sassen and Campbell, 2001; Hoareau et al., 2013) show frequencies of occurrence of about 10–20% in the extratropics; in the tropics the frequency of occurrence is much higher (up to 50%, see e.g. Wang et al., 1996). For these subvisible clouds, a net warming is almost certain, since the albedo effect is almost negligible. Our knowledge about subvisible cirrus clouds is quite limited. Since the ice crystal number concentration in SVCs is very low, the question about the dominant formation mechanism is still pending. In the cold temperature regime ($T < 235\,\mathrm{K}$) two different formation mechanisms are generally possible, namely heterogeneous nucleation at solid aerosol particles (Hoose and Möhler, 2012) and homogeneous freezing of aqueous solution droplets (Koop et al., 2000). For subvisible cirrus Kärcher and Solomon (1999) claimed that both nucleation mechanisms might be possible; in contrast, Jensen et al. (2001) and Froyd et al. (2010) clearly suggested that the dominant mechanism should be heterogeneous nucleation. However, analytical investigations by Kärcher (2002) indicated that also homogeneous nucleation might be possible, although in this study sedimentation of ice crystals was not explicitly included in the model.

In the present study we focus on the formation of SVCs by homogeneous freezing of aqueous solution droplets (short: homogeneous nucleation). We study the formation and evolution of SVCs in an air parcel, which is lifted in slow vertical upward motions ($w \leq 0.05\,\mathrm{ms}^{-1}$), as typical for synoptic scale motions in the extratropics (e.g. along warm fronts, see Kemppi and Sinclair, 2011) or in slow ascent regions in the tropics, as e.g. driven by Kelvin waves (Immler et al., 2008). We include the relevant processes for ice microphysics, i.e. ice nucleation, ice crystal growth due to diffusion of water vapour and sedimentation of ice crystals, respectively. The model is developed on the basis of an evolution equation for mass distributions of ice crystals, including description of microphysical processes based on former work (Spichtinger and Gierens, 2009). However, for using the powerful theory of dynamical systems for analysing the model, we make use of some appropriate simplifications in order to obtain an autonomous system of ordinary differential equations; the variables of

Nonlin. Processes Geophys. Discuss., doi:10.5194/npg-2015-78, 2016
Manuscript under review for journal Nonlin. Processes Geophys.
Published: 19 January 2016

Nonlinear Processes in Geophysics
Discussions
Open Access
EGU

the systems are ice crystal mass and number concentration, respectively, as well as relative humidity with respect to ice.

In section 2 we describe the development of the model, as derived from a more general approach for mass distributions. The results of the numerical integration as well as the mathematical analysis are presented in section 3. Here, we also present comparisons with more complex models and observations. Finally, we draw some conclusions and give an outlook to future work.

2 Model

In this section we describe the development of a simple model, which is used for analytical and numerical investigations. We include the relevant processes for ice clouds in the temperature regime $T < 235\,\mathrm{K}$, namely ice nucleation, diffusional growth and sedimentation, respectively.

We start with the description of an ensemble of ice particles forming a cloud; for this purpose we use a mass distribution $f(m,\boldsymbol{x},t)$ with mass of particles, m, as internal coordinate and space, $\boldsymbol{x}$, and time, t, as external coordinates. (Notation follows the convention in population dynamics, see e.g. Ramkrishna, 2000). The procedure is similar to the derivation by Seifert and Beheng (2006) and Beheng (2010). We investigate a test volume with a certain fixed mass of dry air, therefore f has units $[f] = \mathrm{kg}^{-1}$. Thus, we can formulate the evolution equation for f in a Boltzmann-type way:

$$\frac{\partial(\rho f)}{\partial t} + \nabla_x \cdot (\rho \boldsymbol{u} f) + \frac{\partial(\rho g f)}{\partial m} = \rho h. \tag{1}$$

Here, ρ denotes density of air, $\boldsymbol{u}$ and g are the advection velocities in space and phase space of the internal coordinate and h represents sources and sinks for particles. Note, that all functions $\boldsymbol{u}$, g, h, generally depend on the full set of variables $(m,\boldsymbol{x},t)$.

For the motion of the inertial system we assume a fluid velocity $\boldsymbol{v} = \boldsymbol{v}(\boldsymbol{x},t)$, which is determined by the underlying hydrodynamic motion, governed by some versions or approximations of Navier-Stokes equation. In addition, a single cloud particle might experience a diffusion velocity $\boldsymbol{v}' = \boldsymbol{v}'(m,\boldsymbol{x},t)$ relative to $\boldsymbol{v}$. The total velocity $\boldsymbol{u}$ is thus given by

$$\boldsymbol{u}(m,\boldsymbol{x},t) = \boldsymbol{v}(\boldsymbol{x},t) + \boldsymbol{v}'(m,\boldsymbol{x},t). \tag{2}$$

Thus, we can reformulate equation (2) as follows:

$$\frac{\partial(\rho f)}{\partial t} + \nabla_x \cdot (\rho \boldsymbol{v} f) + \nabla_x \cdot (\rho \boldsymbol{v}' f) + \frac{\partial(\rho g f)}{\partial m} = \rho h. \tag{3}$$

We have to state here that (even with this simplification) we will not be able to derive a general solution for $f(m,\boldsymbol{x},t)$. However, since we are interested in bulk quantities as number and mass concentrations, we use the definition of the general moments of $f(m,\boldsymbol{x},t)$:

$$\mu_k[m](\boldsymbol{x},t) := \int_0^\infty f(m,\boldsymbol{x},t)\, m^k \,\mathrm{d}m, \qquad k \in \mathbb{R}. \tag{4}$$

Nonlin. Processes Geophys. Discuss., doi:10.5194/npg-2015-78, 2016
Manuscript under review for journal Nonlin. Processes Geophys.
Published: 19 January 2016

Nonlinear Processes in Geophysics
Discussions
Open Access
EGU

A bounded mass distribution is uniquely determined by all its integer moments (see e.g. Feller, 1971). For deriving equations for the evolution of moments, we multiply equation (3) by m^k and integrate by parts, using $f(0,\boldsymbol{x},t)=0$ and $f(m,\boldsymbol{x},t)\to 0$ for $m\to\infty$, which are physically reasonable assumptions. Thus, we end with the following equation:

$$\frac{\partial(\rho\mu_k)}{\partial t}+\nabla_x\cdot(\rho\boldsymbol{v}\mu_k)+\nabla_x\cdot\left(\int_0^\infty m^k\rho\boldsymbol{v}' f\,\mathrm{d}m\right)= k\int_0^\infty m^{k-1}\rho g f\,\mathrm{d}m+\int_0^\infty m^k\rho h\,\mathrm{d}m,\qquad k\in\mathbb{R}. \quad (5)$$

The moments are not restricted to $k\in\mathbb{N}$, instead we allow generalized moments with $k\in\mathbb{R}_{\geq 0}$. Formally, the unit of the k-th moment is $\mathrm{kg}^k\mathrm{kg}^{-1}$.

Since we are interested in processes on cloud scale, we can neglect horizontal diffusion velocities; the remaining relative components of $\boldsymbol{v}'$ are determined by sedimentation of particles, i.e. $\boldsymbol{v}'=(v_1',v_2',v_3')=(0,0,v_3')$ and $v_3'=v_3'(m,\boldsymbol{x},t)$. For simplicity, we assume that the gravitational acceleration of ice particles is very quickly balanced by friction of air, thus we can assume that v_3' is represented by the terminal velocity of an ice particle with mass m, i.e. $v_3'=v_t(m)$. We can include this simplification in the following way:

$$\underbrace{\frac{\partial(\rho\mu_k)}{\partial t}+\nabla_x\cdot(\rho\boldsymbol{v}\mu_k)}_{\text{time evolution + advection}}=\underbrace{-\frac{\partial}{\partial z}\left(\int_0^\infty m^k\rho v_t f\,\mathrm{d}m\right)}_{\text{sedimentation}} \underbrace{+k\int_0^\infty m^{k-1}\rho g f\,\mathrm{d}m}_{\text{growth/evaporation}} \underbrace{+\int_0^\infty m^k\rho h\,\mathrm{d}m}_{\text{particle formation/elimination}}. \quad (6)$$

We make the usual ansatz for a double moment scheme, i.e. $k=0,1$ leading to two prognostic equations for number concentration $N_c=\mu_0$ and mass concentration $q_c=\mu_1$:

$$\frac{\partial(\rho\mu_0)}{\partial t}+\nabla_x\cdot(\rho\boldsymbol{v}\mu_0) =-\underbrace{\frac{\partial}{\partial z}\left(\int_0^\infty \rho v_t f\,\mathrm{d}m)\right)}_{SED_n}+\underbrace{\int_0^\infty \rho h\,\mathrm{d}m}_{NUC_n}, \quad (7a)$$

$$\frac{\partial(\rho\mu_1)}{\partial t}+\nabla_x\cdot(\rho\boldsymbol{v}\mu_1)= \underbrace{-\frac{\partial}{\partial z}\left(\int_0^\infty m\rho v_t f\,\mathrm{d}m)\right)}_{SED_q}+\underbrace{\int_0^\infty \rho g f\,\mathrm{d}m}_{DEP_q}+\underbrace{\int_0^\infty m\rho h\,\mathrm{d}m}_{NUC_q}. \quad (7b)$$

Nonlin. Processes Geophys. Discuss., doi:10.5194/npg-2015-78, 2016
Manuscript under review for journal Nonlin. Processes Geophys.
Published: 19 January 2016

Nonlinear Processes in Geophysics
Discussions
Open Access
EGU

Note the units of N_c and q_c relative to the mass of dry air $\left([N_c] = \mathrm{kg}^{-1}, [q_c] = \mathrm{kgkg}^{-1}\right)$.

Now we will address the different terms in equations (7) in more details. First, we have to specify the mass concentration in order to close the system of two moment equations mathematically.

2.1 Choice of distribution

We prescribe a fixed type of mass distribution for the ice crystals, namely a lognormal-distribution of the following form is considered:

$$f(m,t) = \frac{N_c(t)}{\sqrt{2\pi}\log\sigma_m}\exp\left(-\frac{1}{2}\left(\frac{\log(\frac{m}{m_m})}{\log\sigma_m}\right)^2\right)\frac{1}{m}, \tag{8}$$

with the geometric mean mass m_m and the geometric standard deviation σ_m.

For this special distribution the k-th moment is given by

$$\begin{aligned}\mu_k[m] &= N_c m_m^k \exp\left(\frac{1}{2}\left(k\log\sigma_m\right)^2\right)\\ &= N_c \bar{m}^k r_0^{\frac{k(k-1)}{2}} = N_c^{-k} q_c^k r_0^{\frac{k(k-1)}{2}}.\end{aligned} \tag{9}$$

Here, we use the definition of the dimensionless parameter

$$r_0 = \frac{\mu_2\mu_0}{\mu_1^2} = \exp\left(\left(\log(\sigma_m)\right)^2\right) \tag{10}$$

for closing the set of equations. This parameter can also be formulated in terms of the "predominant mass" $m_{pre} = \mu_2/\mu_1$ (Spichtinger and Gierens, 2009; Höller, 1986). In the following r_0 is assumed to be constant. Among others Spichtinger and Gierens (2009) suggest a value of $r_0 = 3$, corresponding to a geometric standard deviation $\sigma_m \approx 2.85$.

2.2 Nucleation

For the formation of ice crystals we exclusively consider homogeneous freezing of aqueous solution droplets (e.g. Koop, 2004). Supercooled solution droplets freeze spontaneously with a nucleation rate J. Similar as for ice particles we can describe the ensemble of solution droplets by a size distribution $f_a = f_a(r)$, where r denotes the radius. Again, we set $[f_a] = \mathrm{kg}^{-1}$ and f_a is normalised by the total number concentration of aerosol particles, $N_a = \mu_0[r]$.

We model homogeneous freezing as a stochastic process with a rate J. For the change in the size distribution $f_a(r)$ we can formulate the following equation (acc. to Seifert and Beheng, 2006) Assuming J as a volume rate (i.e. $[J] = \mathrm{m}^{-3}\mathrm{s}^{-1}$):

$$\left.\frac{\partial(\rho f_a(r))}{\partial t}\right|_{\text{freezing}} = -\frac{4}{3}\pi r^3 J \rho f_a(r). \tag{11}$$

Nonlin. Processes Geophys. Discuss., doi:10.5194/npg-2015-78, 2016
Manuscript under review for journal Nonlin. Processes Geophys.
Published: 19 January 2016

Nonlinear Processes in Geophysics
Discussions
Open Access
EGU

Integration of the equation leads to an equation for the total loss of aerosol particles

$$\frac{\partial(\rho N_a)}{\partial t} = -\frac{4}{3}\pi\rho \int_0^\infty r^3 J f_a(r)\,\mathrm{d}r. \tag{12}$$

assuming a bijective relation between ice crystals and aerosol particles, we combine the total gain of ice particles as:

$$\frac{\partial(\rho N_c)}{\partial t} = -\frac{\partial(\rho N_a)}{\partial t} = \frac{4}{3}\pi\rho \int_0^\infty r^3 J f_a(r)\,\mathrm{d}r = \frac{4}{3}\pi\rho J \mu_{3,a}[r], \tag{13}$$

where $\mu_{3,a}$ denotes the third moment of the size distribution of solution droplets. Here, we assume that $\partial J/\partial r = 0$, thus we can treat the integral as a constant.

Since only a minor fraction of solution droplets is converted to ice, we can assume that the size distribution will be constant in time. Thus, the third moment can be calculated as a constant, given by the type and parameters of $f_a(r)$. We assume $f_a(r)$ as a lognormal distribution with a modal radius of $r_m = 100\,\mathrm{nm}$, a geometric standard deviation $\sigma_r = 1.5$ and a total number concentration $\rho N_a = 3 \times 10^8 \mathrm{m}^{-3}$. Koop et al. (2000) give a parameterisation for the nucleation rate coefficient J as a function of $\Delta a_w := a_w - a_w^i$ (Koop et al., 2000, Table 1, eq. 7). Here a_w is the water activity of the solution and a_w^i is the water activity of the solution in equilibrium with ice. Note, that the freezing characteristics of the droplets do not depend on the chemical composition. By definition the water activity is the ratio e_{sol}/e_{liq} of the vapor pressure over a solution, e_{sol}, and pure liquid water, e_{liq}. Neglecting the Kelvin effect and assuming that the solution droplets are in equilibrium with the environment ($e = e_{sol}$), the water activity is proportional to the water activity in equilibrium with ice, which is the ratio of the water vapour pressure over ice and pure liquid water:

$$a_w = \frac{e_{sol}}{e_{liq}} = \frac{e}{e_{liq}} = \frac{RH_i}{100\%}\frac{e_i}{e_{liq}} = \frac{RH_i}{100\%}\,a_w^i. \tag{14}$$

Both e_i and e_{liq}, only depend on temperature and are parameterised according to Murphy and Koop (2005, eq. 7 and 10, respectively). Hence, Δa_w is a function of RH_i and T, as given by

$$\begin{aligned}\Delta a_w(T, RH_i) &= \left(\frac{RH_i}{100\%} - 1\right) a_w^i(T) \\ &= \left(\frac{RH_i}{100\%} - 1\right) \frac{e_i}{e_{liq}}.\end{aligned} \tag{15}$$

Therefore J is also a function of RH_i and T.

The logarithm of the nucleation rate is parameterised by a third order polynomial in Δa_w (Koop et al., 2000, table1, eq. 7):

$$\begin{aligned}\log_{10} J(T, RH_i) = &-906.7 + 8502\,\Delta a_w \\ &- 26924(\Delta a_w)^2 + 29180(\Delta a_w)^3.\end{aligned} \tag{16}$$

Nonlin. Processes Geophys. Discuss., doi:10.5194/npg-2015-78, 2016
Manuscript under review for journal Nonlin. Processes Geophys.
Published: 19 January 2016

Nonlinear Processes in Geophysics
Discussions
Open Access
EGU

With this, we can formulate the two terms for particle generation:

$$NUC_n = \left.\frac{\partial(\rho N_c)}{\partial t}\right|_{NUC} = \frac{4}{3}\pi\rho N_a \rho \exp\left(\frac{1}{2}(3\log\sigma_r)^2\right) J(RH_i, T) \tag{17a}$$

and

$$NUC_q = m_0\, NUC_n, \tag{17b}$$

using a typical droplet mean mass $m_0 = 10^{-15}\,\mathrm{kg}$ in the spirit of the mean value theorem.

2.3 Depositional growth

The growth of ice crystals is dominated by diffusion. The "advection velocity" g in the mass space is given by the growth equation for a single ice crystal; this equation has the following form (see, e.g., Stephens, 1983):

$$g(m) = \frac{\mathrm{d}m}{\mathrm{d}t} = 4\pi C D_v^* \rho (q_v - q_{v,si}) f_v. \tag{18}$$

Here, $q_{v,s} = \varepsilon\, p_{si}(T)/p$ denotes the saturation mixing ratio, the shape of the ice crystal is accounted for by the capacity C (assuming the electrostatic analogy, see e.g. McDonald, 1963; Jeffreys, 1918), D_v^* is the full diffusion constant including the kinetic correction for small particles (Lamb and Verlinde, 2011) and f_v denotes the ventilation coefficient.

In this study we make use of the following simplifications:

1. Latent heat release at the crystal surface is neglected and the temperature of the ice particles is assumed to be equal to temperature of ambient air.

2. We neglect kinetic corrections, since we are mostly interested in growth of larger crystals. Thus, we can assume

$$D_v^* \approx D_v = D_0 \left(\frac{T}{T_0}\right)^{\alpha} \left(\frac{p_0}{p}\right), \tag{19}$$

with $D_0 = 2.11 \cdot 10^{-5}\,\mathrm{m^2 s^{-1}}$, $T_0 = 273.15\,\mathrm{K}$, $p_0 = 101325\,\mathrm{Pa}$, $\alpha = 1.94$ (e.g. Pruppacher and Klett, 1997).

3. We neglet correction of ventilation, setting $f_v = 1$. Since ventilation correction is relevant for very large crystals, this is a reasonable assumption.

4. The shape of ice crystals, is assumed to be prolate spheroids with a length and an eccentricity ε', this leads to the following expression (McDonald, 1963):

$$C = L \frac{\varepsilon'}{\log\left(\frac{1+\varepsilon'}{1-\varepsilon'}\right)}. \tag{20}$$

Nonlin. Processes Geophys. Discuss., doi:10.5194/npg-2015-78, 2016
Manuscript under review for journal Nonlin. Processes Geophys.
Published: 19 January 2016

Nonlinear Processes in Geophysics
Discussions
Open Access
EGU

For the mass-size relation we assume a simple power law $L(m) = C_i m^{\alpha_i}$ using $C_i = 1.02\,\mathrm{m}$, $\alpha_i = 0.4$, which was fitted to the more complex description in Spichtinger and Gierens (2009), where a transition between droxtals and columns is formulated and used.

The fraction in equation (20) only depends weakly on the crystal mass and can be approximated by a constant mean value of $1/3$. This yields

$$C = \frac{1}{3} C_i m^{\alpha_i}. \tag{21}$$

Thus, we end with the simplified expression for $g(m)$:

$$\begin{aligned} g(m) &\approx \frac{4}{3}\pi C_i m^{\alpha_i} \rho (q_v - q_{v,si}) \\ &= \frac{4}{3}\pi C_i m^{\alpha_i} \rho q_{v,si} (S_i - 1), \end{aligned} \tag{22}$$

using the saturation ratio $S_i = p_v / p_{si}$ and the saturation mixing ratio

$$q_{v,si}(T,p) = \frac{\varepsilon\, p_{si}(T)}{p}. \tag{23}$$

Thus, we can derive the term DEP_q in equation (7b) by integration, i.e.:

$$\begin{aligned} DEP_q &= \int_0^\infty \rho g(m) f(m)\,\mathrm{d}m \\ &= \frac{4}{3}\pi C_i \rho q_{v,si} (S_i - 1) \mu_{a_i}[m] \\ &= \frac{4}{3}\pi C_i \rho q_{v,si} (S_i - 1) n_c^{1-\alpha_i} q_c^{\alpha_i} r_0^{\frac{\alpha_i(\alpha_i-1)}{2}}. \end{aligned} \tag{24}$$

2.4 Sedimentation

For the derivation of the terms SED_q, SED_n we use the mean value theorem for describing the relevant integrals in equation (6) as follows:

$$\int_0^\infty v_t(m) \rho m^k f(m)\,\mathrm{d}m = \bar{v}_k \int_0^\infty \rho m^k f(m)\,\mathrm{d}m = \rho \bar{v}_k \mu_k. \tag{25}$$

Thus, we can describe the weighted terminal velocity $\bar{v}_k$ for the flux of the k-th moment as

$$\bar{v}_k = \frac{1}{\mu_k} \int_0^\infty v_t(m) m^k f(m)\,\mathrm{d}m. \tag{26}$$

Here, we use a simple power law for the representation of the terminal velocity in addition with a density correction term $c(T,p)$, i.e.:

$$v_t(m) = \gamma m^\delta c(T,p) \tag{27}$$

Nonlin. Processes Geophys. Discuss., doi:10.5194/npg-2015-78, 2016
Manuscript under review for journal Nonlin. Processes Geophys.
Published: 19 January 2016

where

$$c(T,p) = \left(\frac{p}{p_{00}}\right)^{a_i} \left(\frac{T}{T_{00}}\right)^{a_2}, \tag{28}$$

$T_{00} = 233\,\mathrm{K}$, $p_{00} = 300\,\mathrm{Pa}$, $a_1 = -0.178$, $a_2 = -0.397$ (see e.g. Spichtinger and Gierens, 2009) and $\gamma = 63292.36\,\mathrm{ms}^{-1}\mathrm{kg}^{-\delta}$, $\delta = 0.57$. Thus, we obtain the weighted velocities for number and mass flux, respectively, in the following form:

$$\bar{v}_0 = \bar{v}_n = \gamma \frac{\mu_\delta}{\mu_0} c(T,p), \tag{29a}$$

$$\bar{v}_1 = \bar{v}_q = \gamma \frac{\mu_{\delta+1}}{\mu_1} c(T,p). \tag{29b}$$

We can formulate the general terms for sedimentation in the moment equations (7):

$$SED_n = \frac{\partial}{\partial z}\left(\rho \bar{v}_n N_c\right) = \frac{\partial}{\partial z}\left(\rho\gamma\mu_{\delta+1}[m]c(T,p)\right) \tag{30a}$$

$$SED_q = \frac{\partial}{\partial z}\left(\rho \bar{v}_q q_c\right) = \frac{\partial}{\partial z}\left(\rho\gamma\mu_{\delta}[m]c(T,p)\right). \tag{30b}$$

2.5 Additional settings

In order to formulate a consistent but simplified system of differential equations we make the following assumptions:

1. Instead of an Eulerian point of view we change to a Lagranian viewpoint , i.e. the Eularian time evolution and advection in the fluid motion,

   $$\frac{\partial(\rho\phi)}{\partial t} + \nabla_x \cdot \left(\rho \boldsymbol{v} \phi\right), \tag{31}$$

   can be seen as total time derivative $\frac{\mathrm{d}(\rho\phi)}{\mathrm{d}t}$. Note that motions relative to the Lagranian evolution are still included, i.e. sedimentation still plays a role.

   We will generally focus on the development inside a prescribed parcel, thus the Langranian description is adequate. We will exclusively consider vertical motions of the air parcel as driven by a vertical velocity component w, i.e. $\boldsymbol{v} = (0,0,w(t))$. Vertical motion of the air parcel will lead to adiabatic processes, i.e. compression or expansion, leading to temperature/pressure changes $\frac{\mathrm{d}T}{\mathrm{d}t}$, $\frac{\mathrm{d}p}{\mathrm{d}t}$ assuming hydrostatic balance, we can explicitly describe the temperature/pressure rates:

   $$\frac{\mathrm{d}T}{\mathrm{d}t} = \frac{\mathrm{d}T}{\mathrm{d}z}\frac{\mathrm{d}z}{\mathrm{d}t} = -\frac{g}{cp} w \tag{32}$$

   $$\frac{\mathrm{d}p}{\mathrm{d}t} = \frac{\mathrm{d}p}{\mathrm{d}z}\frac{\mathrm{d}z}{\mathrm{d}t} = -g\rho w. \tag{33}$$

2. In our study, we will exclusively consider very low vertical velocities or vertical changes with limited amplitude. Thus, we can approximately assume that temperature and pressure

Nonlin. Processes Geophys. Discuss., doi:10.5194/npg-2015-78, 2016
Manuscript under review for journal Nonlin. Processes Geophys.
Published: 19 January 2016

Nonlinear Processes in Geophysics
Discussions
Open Access
EGU

are constant. In consequence, we also keep the volume of our air parcel constant and due to the ideal gas law, density remains constant, too. Hence, ρ drops out in equation (1) and all equations derived from it. At an updraught velocity of $w = 2 \cdot 10^{-2}\mathrm{ms}^{-1}$, temperature would decrease by 0.7 K per hour, meaning that after twelve hours the temperature difference would be about 8 K. However, we are not primarily interested in a highly accurate model, but rather a model that is as simple as possible, describes the aspects of the mechanism qualitatively.

Finally, we can use this assumption for approximating the sedimentation terms. We have to consider terms of the form

$$\frac{\partial}{\partial z}\left(\rho \bar{v}_k \mu_k\right) \qquad k = 0, 1, \tag{34}$$

i.e. vertical changes in the sedimentation flux, $j_k = \rho \bar{v}_k, \mu_k$. Since the volume does not change we assume a box with volume $V = A \cdot \Delta z$ with constant vertical extension Δz and constant base area A. The sedimentation flux j_k is perpendicular to the surface of the base area. To avoid a hyperbolic term in our equations, we approximate the vertical change of the flux by centered differences:

$$\begin{aligned}\frac{\partial}{\partial z} j_k &\approx \frac{1}{\Delta z}\left(j_k^{\mathrm{top}} - j_k^{\mathrm{bottom}}\right) \\ &= \frac{1}{\Delta z}\left(\left(\rho \bar{v}_k \mu_k\right)^{\mathrm{top}} - \left(\rho \bar{v}_k \mu_k\right)_k^{\mathrm{bottom}}\right). \end{aligned} \tag{35}$$

We investigate the top layer of a cloud, therefore by definition $j_k^{\mathrm{top}} = 0$. Hence, we can write:

$$SED_n = -\frac{\rho \bar{v}_N \mu_0}{\Delta z} = -\rho\gamma \frac{\mu_\delta}{\Delta z} c(T,p) \tag{36a}$$

$$SED_q = -\frac{\rho \bar{v}_q \mu_1}{\Delta z} = -\rho\gamma \frac{\mu_{\delta+1}}{\Delta z} c(T,p). \tag{36b}$$

Since we are mostly interested in the top cloud layer, where ice nucleation occurs (see, e.g., Spichtinger and Gierens, 2009), we set the thickness of the cloud layer to $\Delta z = 50\,\mathrm{m}$.

To close the systems of differential equations we introduce an evolution equation for relative humidity, starting with the total derivative of $RH_i = pq_v/(\varepsilon p_{si}(T))$:

$$\frac{\mathrm{d}RH_i}{\mathrm{d}t} = \frac{\partial RH_i}{\partial T}\frac{\mathrm{d}T}{\mathrm{d}t} + \frac{\partial RH_i}{\partial p}\frac{\mathrm{d}p}{\mathrm{d}t} + \frac{\partial RH_i}{\partial q_v}\frac{\mathrm{d}q_v}{\mathrm{d}t}. \tag{37}$$

The ascent of the air parcel is purely adiabatic and no diabatic effects are taken into account. Thus, the first two contributions are given by:

$$\frac{\partial RH_i}{\partial T}\frac{\mathrm{d}T}{\mathrm{d}t} = RH_i \frac{M_{air}}{RT^2} L_{ice} \cdot \frac{g}{c_p} w, \tag{38a}$$

$$\frac{\partial RH_i}{\partial p}\frac{\mathrm{d}p}{\mathrm{d}t} = \frac{RH_i}{p} \cdot \rho g w = -RH_i \frac{M_{air}}{RT} g w, \tag{38b}$$

making use of equation (23), the dry adiabatic lapse rate, and the hydrostatic equilibrium. M_{air} is the molar mass of dry air and L_{ice} is the molar heat of sublimation; we use the parameterisation

Nonlin. Processes Geophys. Discuss., doi:10.5194/npg-2015-78, 2016
Manuscript under review for journal Nonlin. Processes Geophys.
Published: 19 January 2016

for L_{ice} by Murphy and Koop (2005). As usual, g denotes the gravitational acceleration and c_p is the isobaric heat capacity of air. Since these two expressions account for the change of RH_i due to adiabatic cooling they are subsumed under $COOL_{RH}$. Note that using assumption 2, we only consider temperature/pressure changes in equation (38), but leave temperature and pressure constant otherwise. Therefore, we do not include the equations for $\mathrm{d}T/\mathrm{d}t$ and $\mathrm{d}p/\mathrm{d}t$ in our ODE system of the model. This approach will be useful for analytical investigations.

The last term in equation (38) represents the sink due to diffusional growth of ice particles and is denoted as DEP_{RH}, i.e.:

$$\begin{aligned} DEP_{RH} &= \frac{\partial RH_i}{\partial q_v}\frac{\mathrm{d}q_v}{\mathrm{d}t} = -\frac{\partial RH_i}{\partial q_v}\frac{\mathrm{d}q_c}{\mathrm{d}t} \\ &= -\frac{\partial RH_i}{\partial q_v}\cdot\frac{1}{\rho}DEP_{RH} \\ &= -\frac{4}{3}\pi\rho D_v C_i (RH_i - 100\%) r_0^{\frac{\alpha_i(\alpha_i-1)}{2}} N_c^{1-\alpha_i} q_c^{\alpha_i} \end{aligned} \tag{39}$$

2.6 System of ODEs

In summary, the full system of the model equations reads:

$$\begin{aligned} \frac{\mathrm{d}N_c}{\mathrm{d}t} &= \frac{4\pi}{3}\frac{n_a}{\rho} r_m^3 \exp\left(\frac{1}{2}(3\ln(\sigma_r))^2\right) J(RH_i, T) \\ &\quad - \frac{\gamma\, c(T,p)}{\Delta z} r_0^{\frac{\delta(\delta-1)}{2}} N_c^{1-\delta} q_c^{\delta} \end{aligned} \tag{40a}$$

$$\begin{aligned} \frac{\mathrm{d}q_c}{\mathrm{d}t} &= m_0 \frac{4\pi}{3}\frac{n_a}{\rho} r_m^3 \exp\left(\frac{1}{2}(3\ln(\sigma_r))^2\right) \\ &\quad \cdot J(RH_i, T) - \frac{\gamma\, c(T,p)}{\Delta z} r_0^{\frac{\delta(\delta+1)}{2}} N_c^{-\delta} q_c^{1+\delta} \\ &\quad + \pi\varepsilon\rho D_v C_i \frac{e_i}{p}\left(\frac{RH_i}{100\%} - 1\right) r_0^{\frac{\alpha_i(\alpha_i-1)}{2}} N_c^{1-\alpha_i} q_c^{\alpha_i} \end{aligned} \tag{40b}$$

$$\begin{aligned} \frac{\mathrm{d}RH_i}{\mathrm{d}t} &= RH_i g w \frac{M_{air}}{RT}\left(\frac{L_{ice}}{c_p T} - 1\right) \\ &\quad - \pi\rho D_v C_i (RH_i - 100\%) r_0^{\frac{\alpha_i(\alpha_i-1)}{2}} N_c^{1-\alpha_i} q_c^{\alpha_i}. \end{aligned} \tag{40c}$$

This is an autonomous system of ordinary differential equations. For better readability the equations are abbreviated:

$$\dot{\boldsymbol{x}} = \boldsymbol{F}(\boldsymbol{x}), \qquad \text{with } \boldsymbol{x} = (N_c, q_c, RH_i)^T, \tag{41}$$

and $\boldsymbol{F}$ the right hand side of (40). Note that the assumption of constant temperature, pressure and vertical velocity ensures that the system (40) possesses critical points.

Nonlin. Processes Geophys. Discuss., doi:10.5194/npg-2015-78, 2016
Manuscript under review for journal Nonlin. Processes Geophys.
Published: 19 January 2016

3 Results

3.1 General features

We examine the system for a range of parameter values $0 < w \leq 0.05\,\mathrm{m\,s^{-1}}$ and $190\,\mathrm{K} \leq T \leq 230\,\mathrm{K}$, at a pressure of $p = 300\,\mathrm{hPa}$, which corresponds to upper tropospheric conditions with moderate vertical motions as in synoptic weather situations or slow upward motions in the tropics (e.g. Kelvin waves). The air parcel is initialized with no ice particles ($N_c(0) = 0$, $q_c(0) = 0$) and at high supersaturation w.r.t. ice ($RH_i(0) = 140\,\%$). The prognostic equations (40) are integrated numerically using the *LSODA* algorithm from the Fortran library *ODEPACK* (Hindmarsh, 1983).

The general cloud formation mechanism works as follows: The adiabatic cooling causes the relative humidity, and thus the nucleation rate, to rise until the freezing probability is high enough to allow ice nucleation. This corresponds merely with a threshold in relative humidity. According to Ren and Mackenzie (2005), this threshold might be expressed as $RH_{i,crit} = (2.349 - T/259)\cdot 100\%$, i.e. $RH_{i,crit} \approx$ 140–150%. The stronger the dynamical forcing w, the stronger the nucleation event and the more ice particles form. Ice particle growth then reduces the relative humidity and hence the freezing rate is also reduced (see equation (37), last term). The crystals, that have become large, fall out, thus sedimentation reduces the ice crystal concentrations, which causes relative humidity to further increase. In fact, sedimentation is the key process, which leads to different states in the cloud evolution. The system exhibits two qualitatively distinct behaviours, depending on the parameter values of w and T.

State 1: At rather high temperatures and slow vertical velocities, the three competing microphysical processes are relatively slow and act on similar time scales so none of them is dominant. In particular, freezing rates are rather small in these cases, therefore only few ice crystals are formed initially. The three processes are more or less in balance, resulting in a damped oscillation in all three variables, finally asymptotically reaching an equilibrium state in numerical integrations of equations (40), as shown in figure 1. Note, that in this state, nucleation is occurring continuously, as relative humidity remains above the freezing threshold at all times and thus the nucleation rates are high enough to produce ice crystals. This results in smooth oscillations instead of sharp nucleation events. If the air parcel is not disturbed and the vertical updraught remains unchanged, the cloud that forms will persist and will have constant microphysical properties. The cloud in the steady state typically contains low crystal concentrations. The dynamic equilibrium remains at high supersaturations, i. e. is far from thermodynamic equilibrium. The cloud properties are discussed quantitatively in section 3.3 in more detail.

State 2: When increasing w or decreasing T, respectively, to a certain level, there is no damping and stationarity is not reached anymore (see figure 2) because the processes are not in balance in this case. Instead, we obtain pulse-like nucleation with distinct nucleation events and the nucleation rates fall far below the critical rates at $RH_{i,crit}$. The amplitude of the oscillation is very large in

Nonlin. Processes Geophys. Discuss., doi:10.5194/npg-2015-78, 2016
Manuscript under review for journal Nonlin. Processes Geophys.
Published: 19 January 2016

all variables and the ice particle concentration is reduced to a small fraction of the maximum value once in a period. At colder temperatures and faster vertical velocities, the nucleation rates are much higher, so freezing is the dominant process in the beginning. After a while, ice crystal growth becomes dominant and when the crystals have become large, sedimentation sets in and crystal numbers decrease rapidly. Finally, the cycle starts over. In this case, the freezing events are clearly separated, as opposed to the first case. In the beginning, the amplitude in the three variables decreases slightly from one event to the next, but after a while, the amplitude stays constant. The system reaches a limit cycle, through which it passes over and over periodically. This kind of scenario was observed in former studies (e.g. Spichtinger and Cziczo, 2010; Kay et al., 2006).

In the following section, we conduct a classical dynamical system analysis of the ODE system (41). Then, we discuss the properties of the modeled cloud and compare it to other models and observations.

3.2 Mathematical analysis

In a first step, the dynamical system (41) can be characterised by its critical points $\boldsymbol{x_0}$, i.e. the values where $\boldsymbol{F}(\boldsymbol{x_0}) = \boldsymbol{0}$. Since the system is autonomous the critical points are equilibrium points. The critical points of the system cannot be determined analytically. However, under the assumption that the nucleation term NUC_q for q_c is negligible (it is several orders of magnitude smaller than the other terms in equation (40b)), it is possible to rearrange the equations (without losing any positive solutions) in a way that only one equation for RH_i has to be solved numerically. The critical values of N_c and q_c can be derived analytically from that. This equation reads:

$$\begin{aligned}&\frac{4\pi}{3}\frac{n_a}{\rho}r_m^3\exp\left(\frac{1}{2}\left(3\ln(\sigma_r)\right)^2\right)J(RH_i,T)\\&=\frac{\gamma c(T,p)gwM_{air}\left(L_{ice}/c_p-1\right)}{\Delta z RT\pi\rho C_i}\cdot r_0^{\frac{\delta}{2}(\delta-1)(\alpha_i-1)-\frac{\alpha_i}{2}(\alpha_i-1)}\\&\qquad\cdot\left(\frac{\pi\epsilon\rho D_v C_i e_i\Delta z}{\gamma c(T,p)p_i}\cdot\left(\frac{RH_i}{100\%}-1\right)\right)^{\delta-\alpha_i}\frac{RH_i}{RH_i-100\%}.\end{aligned}\tag{42}$$

Equation (42) has a unique solution because the left-hand side is a strictly monotonic increasing function of RH_i and the right-hand side is strictly monotonic decreasing. Therefore, there exists a unique critical point, $\boldsymbol{x_0}$, in the relevant domain of the phase space ($RH_i > 100\,\%$, $N_c > 0$, $q_c > 0$).

In order to examine the qualitative behaviour of the solution in a neighbourhood of the equilibrium state, the ODE system is linearised about the critical point $\boldsymbol{x}_0$:

$$\dot{\boldsymbol{x}} = \boldsymbol{F}(\boldsymbol{x_0}) + \mathbf{DF}\big|_{\boldsymbol{x}_0}(\boldsymbol{x}-\boldsymbol{x}_0) + \mathcal{O}(|\boldsymbol{x}-\boldsymbol{x}_0|^2),\tag{43}$$

where $\mathbf{DF}|_{\boldsymbol{x}_0}$ is the Jacobian of $\boldsymbol{F}$ evaluated at the point $\boldsymbol{x}_0$. The three eigenvalues of the Jacobian, $\lambda_1, \lambda_2, \lambda_3$, determine the quality of the critical point (Verhulst, 1996, Chapter 3). The Jacobian of the system has two complex conjugate eigenvalues, λ_1 and λ_2, whose real part can be positive or negative, depending on the parameters, w and T. The third eigenvalue, $\lambda_3 \in \mathbb{R}$, is always negative.

Nonlin. Processes Geophys. Discuss., doi:10.5194/npg-2015-78, 2016
Manuscript under review for journal Nonlin. Processes Geophys.
Published: 19 January 2016

If the real part of the complex conjugate eigenvalues is negative ($\mathrm{Re}(\lambda_1) = \mathrm{Re}(\lambda_2) < 0$), the critical point is a positive attractor in equation (43), which means that a solution that starts in a neighbourhood of $\boldsymbol{x_0}$ will asymptotically converge to $\boldsymbol{x_0}$ (Verhulst, 1996). This corresponds to state 1, i.e. the damped oscillation where the system reaches stationarity. According to the Poincaré-Lyapunov theorem (Verhulst, 1996, theorem 7.1), positive attraction in the linearised system is also valid for the full non-linear system. Therefore, $\boldsymbol{x_0}$ is asymptotically stable and acts as a positive attractor in equation (41) in state 1 (damping state). Figure 3 shows the trajectory of a solution of the system (40) in the 3D phase space, spiralling towards the equilibrium point, i.e. the positive attractor.

In case of undamped oscillation (state 2), the real part of the complex eigenvalues is positive ($\mathrm{Re}(\lambda_1) = \mathrm{Re}(\lambda_2) > 0$).

The transition from positive attractor to limit cycle is a so called Hopf bifurcation (Verhulst, 1996) and is associated with a transition from two conjugate complex eigenvalues with negative real part to two conjugate complex eigenvalues with positive real part, via two purely imaginary eigenvalues. The bifurcation diagram is a line in w-T-space that separates the two regimes positive attraction vs. limit cycle (see figure 5). The bifurcation points were identified numerically using the eigenvalue criterion, $\mathrm{Re}(\lambda_1) = \mathrm{Re}(\lambda_2) = 0$.

The limit cycle was determined numerically by computing the Poincaré map of the system (Argyris et al., 2010; Verhulst, 1996). Choose a two-dimensional plane Σ in the phase space, which is transverse to the trajectory of the solution of equation (41); Σ is called Poincaré section. The sequence of points in the phase space where the trajectory crosses Σ converges numerically to the the point on the limit cycle that is in Σ. Once we find one such point on the limit cycle, we can use it as the initial condition in (41) to compute the complete limit cycle. However, since this method requires numerical integration of equation (41), it is not of further interest for the analytical investigation.

3.3 Discussion of results

In the "attractor" regime, i.e. state 1 of the system, the critical point corresponds to the equilibrium values within the finally persisting cloud. Hence, in this parameter regime, we describe the properties of the modeled cloud by the values of the system variables at the critical point. For the "limit cycle" regime, the critical point does not describe the changing properties of the cloud since it is only in the centre of the periodic orbit and the trajectory does not approach it. A more revealing measure for the cloud properties in this regime is a probability density of the values the variables take in the limit cycle, or at least median, maximum and minimum values.

Figure 6 shows ice crystal mass and number concentrations, respectively, at the critical point, $\boldsymbol{x_0}$, as a function of vertical velocity ($q_c(w)$, $N_c(w)$) for different temperature regimes. The solid lines in both panels correspond to state 1 (attractor regime), whereas the dashed lines indicate the values at the critical point, $\boldsymbol{x_0}$, for state 2 (limit cycle regime); note that for state 2, $\boldsymbol{x_0}$ is an unstable focus.

Nonlin. Processes Geophys. Discuss., doi:10.5194/npg-2015-78, 2016
Manuscript under review for journal Nonlin. Processes Geophys.
Published: 19 January 2016

Nonlinear Processes in Geophysics
Discussions
Open Access
EGU

Ice crystal number concentrations at the critical point take values in the range $3\times10^2\,\mathrm{kg}^{-1} \leq N_c \leq 2\times10^5\ \mathrm{kg}^{-1}$ (figure 6, top), which corresponds to ice crystal number densities of $0.1\,\mathrm{L}^{-1} \leq n_c \leq 110\,\mathrm{L}^{-1}$. Ice crystal mass concentration ranges between $4\times10^{-9} \leq q_c \leq 3\times10^{-6}$ kg kg^{-1} (figure 6, bottom). This corresponds to an ice water content of $2.2\times10^{-9} \leq IWC \leq 1.4\times10^{-6}\,\mathrm{kgm}^{-3}$.

As expected from theory and from former numerical investigations (e.g. Kärcher and Lohmann (2002)), the ice crystal number concentrations display a strong increase with rising vertical velocity. Due to increased crystal growth rates at higher temperatures, N_c decreases with rising T.

In the double logarithmic representation in figure 6, the number concentrations $N_c(w)$ at $\boldsymbol{x_0}$ appear as straight lines. For different temperature regimes, there seems to be a constant shift between the curves $N_c(w)$ (i.e. a constant factor c(T)), leading to parallel lines in the double logarithmic representation.

For the limit cycle regime (state 2), we can still derive the values of mass and number concentrations at the critical point, $\boldsymbol{x_0}$. However, since this point is unstable and is never reached, another representation is needed to describe the range of ice crystal concentrations. As indicated in figures 5 and 6, the limit cycle behaviour occurs for temperatures $T < 230\,\mathrm{K}$ for the investigated updraught regime $0 \leq w \leq 0.05\,\mathrm{ms}^{-1}$. Thus, in figure 7 we represent maximum, median and minimum values for ice crystal number concentrations (dashed lines) in the limit cycle regime for temperatures $T = 190, 200, 210, 220\,\mathrm{K}$. In addition, the ice crystal number concentration at the critical point, $\boldsymbol{x_0}$, is displayed. We observe a large variation in the number concentrations of up to two orders of magnitude. This behaviour is reasonable since sedimentation reduces the amount of ice crystals in a dominant manner, while new ice crystals are formed by nucleation in a pulsating way.

The mass concentration of the ice crystals is largely determined by diffusional growth. As indicated in the model description (section 2), this term depends on temperature and also on number concentration, leading again to an exponential behaviour as represented in figure 6 (bottom) and to a constant factor between the different temperatures, represented as parallel lines.

For the attractor regime, we can directly investigate the mean mass of the ice crystals, $\overline{m} = q_c/N_c$, at $\boldsymbol{x_0}$, which is displayed in figure 8. The variation of $\overline{m}$ at the critical point due to the vertical velocity is marginal, as indicated in the figure. Thus, we can assume that $\overline{m}$ can be approximated by a function of temperature. The mean mass at $\boldsymbol{x_0}$ ranges between $\overline{m} \sim 10^{-12}\,\mathrm{kg}$ and $\overline{m} \sim 2\times10^{-10}\,\mathrm{kg}$, which corresponds to mean sizes between $\overline{L} \sim 16\,\mu\mathrm{m}$ and $\overline{L} \sim 134\,\mu\mathrm{m}$. For the limit cycle regime (state 2), we indicate the variation in the mean mass by box and whiskers plots, displaying the median value (red markers) as well as 25/75% percentiles and minimum/maximum values. Note here that variation of mean mass is usually of one order of magnitude. For cold temperatures the variation is larger due to a higher variability in ice crystal number concentration (see figure 7), whereas the mass concentration in ice clouds is mainly dominated by available water vapour.

Nonlin. Processes Geophys. Discuss., doi:10.5194/npg-2015-78, 2016
Manuscript under review for journal Nonlin. Processes Geophys.
Published: 19 January 2016

3.4 Comparison with other simulations

For comparison with a more complex and realistic model we carry out simulations with the boxmodel as described by Spichtinger & Gierens (2009) and Spichtinger & Cziczo (2010). In the following this model is termed "complex model". We scan through the T-w parameter space using initial temperatures in the range $190 \leq T \leq 235\,\mathrm{K}$ with a temperature increment of $\Delta T = 5\,\mathrm{K}$ and vertical velocities in the range $0.005 \leq w \leq 0.05\,\mathrm{ms}^{-1}$ with a velocity increment of $\Delta w = 0.005\,\mathrm{ms}^{-1}$, leading to 90 simulations. Additionally, we fixed initial conditions $p = 300\,\mathrm{hPa}$ and $RHi = 140\%$. The results of these simulations are very similar to the results of the analytical model.

We can again identify regimes in the T-w parameter space showing the known two different states, i.e. damped oscillations (state 1) and limit cycle behaviour (state 2). In figure 9 the case of damped oscillation is shown in both model simulations. Here, initial temperature of $T = 220\,\mathrm{K}$ is used with a vertical velocity of $w = 0.01\,\mathrm{ms}^{-1}$. Green lines indicate the evolution in the complex model simulation, whereas blue lines represent the evolution in the simple analytical model. Both model simulations agree quite well. For the variables number and mass concentration both models produce almost the same values, however the values for relative humidity are slightly lower for the simple model simulation. In fact, the onset of ice nucleation is shifted between the two models due to differently detailed representation of ice nucleation in both models. This leads to the difference in relative humidity values. Qualitatively, the models agree very well, the oscillation periods are very similar and also the damping is almost the same. Note that the agreement between the models is not always that good for all parameter values; however, the model results for variables ice mass and number concentrations, respectively, always agree within less than one order of magnitude.

For the complex model simulations the environmental conditions change, i.e. temperature and pressure are decreasing due to adiabatic expansion. Thus, no steady state can be reached. The values for ice crystal number concentrations and relative humidity are slightly rising with time in the quasi steady state at the end of the simulation. Ice crystal mass concentration is slightly decreasing. Generally, we can say that for state 1 (damped oscillations) the agreement between the respective two model simulations is very good; this holds for all cases of damped oscillations.

In figure 10 a case of limit cycle behaviour is shown. As in figure 9, green lines indicate the complex model simulations and the simple model results are represented by blue lines, respectively. The initial conditions for both models are given by $T = 210\,\mathrm{K}$ and $w = 0.02\,\mathrm{ms}^{-1}$. Again, we find very good agreement in the cloud variables N_c, q_c between both model simulations. There is again a shift in relative humidity due to the representation of ice nucleation in the different models. The limit cycle behaviour is present in both simulations; qualitatively they also agree very well in terms of the periods of the oscillations. Again, we have to state that the agreement is not always that good in the absolute values of variables as in this represented case. However, qualitatively the limit cycle cases agree very well.

Nonlin. Processes Geophys. Discuss., doi:10.5194/npg-2015-78, 2016
Manuscript under review for journal Nonlin. Processes Geophys.
Published: 19 January 2016

The bifurcation diagram as represented in figure 5 cannot completely be reproduced by the complex simulations. For initial conditions close to the boundary between state 1 and state 2 we observe a different behaviour. Since the complex model includes changes in temperature, the parameters are changed during the simulations. For instance, the simulation starts in the regime of a damped oscillation (e.g. high temperature vales at low updraughts) and the time evolution follows first this (theoretical) kind of time evolution. However, the temperature change leads to a path in the phase diagram (figure 5) and at some stage the boundary between the two states is crossed. Now, a different scenario, namely limit cycle behaviour, should be present. In fact, if the oscillations are not already damped out, we can observe in the simulations that after crossing the bifurcation line in figure 5 the complex model simulations then exhibit a limit cycle behaviour. An example for this situation is given in figure 11. Here, we show a long simulation with the complex model for initial conditions $T = 225\,\mathrm{K}$ and $w = 0.035\,\mathrm{ms}^{-1}$; thus, as shown in the phase diagram (figure 5), the model starts in the regime of damped oscillations. In the time evolution, we can see the damped oscillation very clearly for up to about four hours. At this time, the temperature is about $T \sim 220\,\mathrm{K}$ and according to the phase diagram there is the transition to the limit cycle behaviour. In the further time evolution, the limit cycle behaviour is present, i.e. the oscillations are not damped but in contrast the amplitude in variables N_c, q_c and relative humidity increases slightly. After further cooling, we observe that the period of the oscillations changes as well, since the period of the limit cycle depends on environmental conditions. Thus, we can conclude that for realistic simulations including changes in environmental conditions there could be transitions between the theoretically determined states. However, the behaviour of the actual states can still be explained by the phase diagram as obtained from our analytical considerations.

Comparison with theoretical results by Kärcher (2002) shows good agreement as well. Actually, in our investigations with the simple analytical model we found low ice crystal number concentrations similar to results by Kärcher (2002); the dependence of number concentrations on w and T also agrees very well with analytical considerations by Kärcher (2002). However, our approach goes beyond the results by Kärcher (2002) since we allow for sedimentation of ice crystals. This additional process leads to the oscillatory behaviour in both cases, the damped oscillation in the attractor case (state 1) as well as the undamped oscillation in the limit cycle case (state 2). Especially the continuous nucleation in the state 1 scenario (damped oscillation) is only possible if we allow for sedimentation of ice crystals. Otherwise, the nucleation event would stop after depositional growth has reduced the supersaturation such that nucleation rates become negligible. Thus, we can state that our scenarios might be more realistic, although the microphysical poperties in both studies are quite similar.

Nonlin. Processes Geophys. Discuss., doi:10.5194/npg-2015-78, 2016
Manuscript under review for journal Nonlin. Processes Geophys.
Published: 19 January 2016

Nonlinear Processes in Geophysics
Discussions
Open Access
EGU

3.5 Comparison with observations

For comparison with observations we focus on in situ measurements of ice crystals in subvisible cirrus clouds. Since it is very difficult to measure low number concentrations, only few measurement studies are available. We compare our results with measurements by Kübbeler et al. (2011), Lawson et al. (2008) and Davis et al. (2010).

Our model results lead to ice crystal number concentrations in the range $0.1\,\mathrm{L}^{-1} \leq \rho N_c \leq 110\,\mathrm{L}^{-1}$ and mean ice crystal sizes in the range $\sim 16\,\mu\mathrm{m} \leq \overline{L} \leq 134\,\mu\mathrm{m}$. Note, that the variation in number concentrations span over three orders of magnitude and the variation in mean sizes is still within two orders of magnitude. These values agree quite well with the measurements. Kübbeler et al. (2011) indicated quite high number concentrations in order of $\sim 100\,\mathrm{L}^{-1}$ for small ice crystals ($L \sim 10\,\mu\mathrm{m}$) but quite low number concentrations $0.1 \leq \rho N_c \leq 10\,\mathrm{L}^{-1}$ for large ice crystals (equivalent radius $r > 50\,\mu\mathrm{m}$). Lawson et al. (2008) reported ice crystal number concentrations in the range $22.5 \leq \rho N_c \leq 188.8\,\mathrm{L}^{-1}$ with mean value and standard deviation $66 \pm 30.8\,\mathrm{L}^{-1}$ for ice crystals in the size range $1 \leq L \leq 200\,\mu\mathrm{m}$. Finally, Davis et al. (2010) reported very low ice crystal number concentrations with a mean value of $2\,\mathrm{L}^{-1}$ and mean sizes of $14\,\mu\mathrm{m}$ during the tropical measurement campaign TC4. However, in their study values from former measurement campaigns are reported to be in the range $10 \leq \rho N_c \leq 100\,\mathrm{L}^{-1}$ and for effective radii $10 \leq r \leq 20\,\mu\mathrm{m}$. Overall we can state that regarding the high spread in the measurements our results from a simple analytical model agree quite well with in situ measurements.

Actually, from in situ measurements, which constitute an Eulerian point of view by definition, we cannot decide in which of the possible states (attractor regime vs. limit cycle) the observed cloud might be. We also have to keep in mind that in reality the motion of air parcels might be disturbed by small scale turbulence or other dynamical effects.

4 Conclusions

In this study we develop an analytical model for describing subvisible cirrus clouds in the tropopause region from first principles starting with a Boltzmann-type equation for the evolution of a cloud mass distribution. The model consists of a set of ordinary differential equations for the variables ice crystal mass and number concentration as well as relative humidity with respect to ice. The model contains the relevant cloud processes ice nucleation, diffusional growth and sedimentation, respectively. The forcing terms are non-linear and the whole system is autonomous. We use this model for numerical simulations as well as for mathematical analysis, applying theory of dynamical systems. In the analysis we can show that there are two qualitatively different states in the long-term evolution of the model. The two states are (a) a positive attractor and (b) a limit cycle for the cloud variables. Thus, we find a Hopf bifurcation, which is characterized by the change of the real part of the two conjugate-complex eigenvalues from negative values to positive values via two purely

Nonlin. Processes Geophys. Discuss., doi:10.5194/npg-2015-78, 2016
Manuscript under review for journal Nonlin. Processes Geophys.
Published: 19 January 2016

imaginary eigenvalues. The transition between the states is determined by the parameters vertical velocity w and environmental temperature T.

The microphysical properties of the cloud in both states are similar and depend mostly on the environmental conditions as vertical velocity and temperature. However, for the limit cycle case the spread in ice crystal mass and number concentration is obviously larger than in the attractor case. For the equilibrium point the mean mass depends only slightly on vertical velocity, thus we can approximate the mean mass as a function of temperature.

The comparison with a complex boxmodel by Spichtinger and Gierens (2009) shows very good agreement. In fact, the qualitative behaviour as determined for the analytical model can also be found for the complex model simulations. Also in a quantitative way both models agree quite well.

Comparison with former analytical investigations by Kärcher (2002) shows also good agreement with our model. However, since we include sedimentation in our model, our results go clearly beyond the former investigations; the long-term behaviour is different, since the inclusion of sedimentation crucially leads to the bifurcation, depending on environmental conditions.

Since there are only a few in situ measurements of subvisible cirrus available, it is quite difficult to carry out solid comparisons. However, we try to compare with measurements as described by Kübbeler et al. (2011), Lawson et al. (2008), and Davis et al. (2010) and find good agreement with our results.

Thus, we can summarize that homogeneous freezing of aqueous solution droplets at low temperatures ($T < 235\,\mathrm{K}$) might be a possible candidate for formation of ice crystals und slow updraught conditions, leading to very thin or subvisible cirrus clouds. The final state of the cloud in the long-term behaviour is very similar for both cases. Therefore, we cannot decide from values of microphysical properties in a certain range in which state the cloud might be. Even if we had more measurements, we probably would not be able to decide between the two states just using the Eulerian measurements without a Lagrangian point of view.

Finally, we can state that we could develop a meaningful minimal model for describing the main features of subvisible cirrus clouds. Former investigations using boxmodels indicated that there might be different regimes in the behaviour of the clouds for longer simulation times. For instance, in studies by Kay et al. (2006) and Spichtinger and Cziczo (2010) oscillatory behaviours as well as attractors could be seen. However, only a detailed mathematical analysis could show that there is a bifurcation in the long-term behaviour and that it depends mostly on environmental parameters as updraught velocity and temperature. This analysis was only possible, since we developed an analytical model, which is close enough to complex models but is also simple enough for mathematical analysis.

The determined Hopf bifurcation in addition with the two different states show that clouds might show inherent structures, which are crucially determined by the microphysical cloud processes themselves in addition to environmental conditions. Similar structure formation was already seen in ana-

Nonlin. Processes Geophys. Discuss., doi:10.5194/npg-2015-78, 2016
Manuscript under review for journal Nonlin. Processes Geophys.
Published: 19 January 2016

lytical cloud models for liquid and mixed-phase clouds as developed by Wacker (1992, 1995, 2006) or Hauf (1993). Investigations and analysis of the microphysical processes in terms of sets of ordinary differential equations are a first but urgently necessary step in order to investigate structure formation inside clouds. Once we understand the possible structures in clouds as determined by microphysics, we can proceed further in order to investigate further structure formation as driven by diffusion processes and others, leading to spatial structures of clouds.

Last but not least we would like to note that simple models as the derived minimal model of subvisible cirrus clouds might also serve as prototypes for new generation of cloud parameterisations in large-scale models; since these models describe the structure of clouds in terms of cloud variables and environmental conditions, these models might be used for describing such structures embedded into a coarse grid model. However, further research in this direction is necessary in order to proceed from pure model prototypes to meaningful cloud parameterisations.

Acknowledgements. We thank M. Baumgartner, M. C. Götze, L. Grüne and R. Klein for fruitful discussions. This study was prepared with support by the German "Bundesministerium für Bildung und Forschung (BMBF)" within the HD(CP)^2 initiative, project S4 (01LK1216A) and with support by the German Research Foundation (DFG) within the TransRegio 165 "waves to weather", project A2 (SP 1163/6-1).

Nonlin. Processes Geophys. Discuss., doi:10.5194/npg-2015-78, 2016
Manuscript under review for journal Nonlin. Processes Geophys.
Published: 19 January 2016

Nonlinear Processes in Geophysics
Discussions
Open Access
EGU

References

Argyris, J., Faust, G., Haase, M., and Friedrich, R.: Die Erforschung des Chaos, Springer, 2010.

Beheng, K. D.: The Evolution of Raindrop Spectra: A Review of Microphysical Essentials., in: Rainfall: State of the Science., edited by Testik, F. Y. and Gebremichael, M., vol. 191 of *Geophysical Monograph Series*, pp. 29–48, American Geophysical Union, Washington, USA, doi:10.1029/2010GM000957, 2010.

Chen, T., Rossow, W. B., and Zhang, Y.: Radiative effects of cloud-type variations, Journal of climate, 13, 264–286, 2000.

Davis, S., Hlavka, D., Jensen, E., Rosenlof, K., Yang, Q., Schmidt, S., Borrmann, S., Frey, W., Lawson, P., Voemel, H., and Bui, T. P.: In situ and lidar observations of tropopause subvisible cirrus clouds during TC4, Journal of Geophysical Research: Atmospheres, 115, D00J17, doi:10.1029/2009JD013093, http://dx.doi.org/10.1029/2009JD013093, 2010.

Feller, W.: An Introduction to Probability Theory and Its Applications, no. Bd. 2 in An Introduction to Probability Theory and Its Applications, Wiley, Chichester, UK, 1971.

Froyd, K., Murphy, D., Lawson, P., Baumgardner, D., and Herman, R.: Aerosols that form subvisible cirrus at the tropical tropopause, Atmospheric Chemistry and Physics, 10, 209–218, 2010.

Hauf, T.: Microphysical kinetics in phase space: The warm rain process, Atmospheric Research, 29, 55 – 84, doi:http://dx.doi.org/10.1016/0169-8095(93)90037-O, http://www.sciencedirect.com/science/article/pii/016980959390037O, 1993.

Hindmarsh, A. C.: ODEPACK, A Systematized Collection of ODE Solvers, in: Scientific Computing, edited by Stepleman, R. S., pp. 55.–64, North-Holland, 1983.

Hoareau, C., Keckhut, P., Noel, V., Chepfer, H., and Baray, J.-L.: A decadal cirrus clouds climatology from ground-based and spaceborne lidars above the south of France (43.9° N–5.7° E), Atmospheric Chemistry and Physics, 13, 6951–6963, 2013.

Hoose, C. and Möhler, O.: Heterogeneous ice nucleation on atmospheric aerosols: a review of results from laboratory experiments, Atmospheric Chemistry and Physics, 12, 9817–9854, doi:10.5194/acp-12-9817-2012, http://www.atmos-chem-phys.net/12/9817/2012/, 2012.

Höller, H.: Parameterization of cloud-microphysical processes in a three-dimensional convective mesoscale model, Tech. rep., Deutsche Forschungs- und Versuchsanstalt für Luft- und Raumfahrt, 1986.

Immler, F., Krüger, K., Fujiwara, M., Verver, G., Rex, M., and Schrems, O.: Correlation between equatorial Kelvin waves and the occurrence of extremely thin ice clouds at the tropical tropopause, Atmospheric Chemistry and Physics, 8, 4019–4026, doi:10.5194/acp-8-4019-2008, http://www.atmos-chem-phys.net/8/4019/2008/, 2008.

Jeffreys, H.: Some Problems of Evaporation, The London, Edinburgh, and Dublin Philosophical Magazine and Journal of Science, 35, 270–280, 1918.

Jensen, E. J., Toon, O. B., Vay, S. A., Ovarlez, J., May, R., Bui, T. P., Twohy, C. H., Gandrud, B. W., Pueschel, R. F., and Schumann, U.: Prevalence of ice-supersaturated regions in the upper troposphere: Implications for optically thin ice cloud formation, Journal of Geophysical Research: Atmospheres, 106, 17 253–17 266, doi:10.1029/2000JD900526, http://dx.doi.org/10.1029/2000JD900526, 2001.

Kärcher, B.: Properties of subvisible cirrus clouds formed by homogeneous freezing, Atmospheric Chemistry and Physics, 2, 161–170, 2002.

Kärcher, B. and Lohmann, U.: A parameterization of cirrus cloud formation: Homogeneous freezing including effects of aerosol size, Journal of Geophysical Research, 107, 4010, doi:10.1029/2001JD000470, 2002.

Kärcher, B. and Solomon, S.: On the composition and optical extinction of particles in the tropopause region, Journal of Geophysical Research: Atmospheres, 104, 27 441–27 459, doi:10.1029/1999JD900838, http://dx.doi.org/10.1029/1999JD900838, 1999.

Kay, J. E., Baker, M., and Hegg, D.: Microphysical and dynamical controls on cirrus cloud optical depth distributions, Journal of Geophysical Research: Atmospheres, 111, n/a–n/a, doi:10.1029/2005JD006916, http://dx.doi.org/10.1029/2005JD006916, d24205, 2006.

Kemppi, M. L. and Sinclair, V. A.: Structure of a warm front: Helsinki testbed observations and model simulation, Monthly Weather Review, 139, 2876–2900, 2011.

Koop, T.: Homogeneous ice nucleation in water and aqueous solutions, Zeitschrift für Physikalische Chemie/International journal of research in physical chemistry and chemical physics, 218, 1231–1258, 2004.

Koop, T., Luo, B., Tsias, A., and Peter, T.: Water activity as the determinant for homogeneous ice nucleation in aqueous solutions, Nature, 406, 611–614, 2000.

Kübbeler, M., Hildebrandt, M., Meyer, J., Schiller, C., Hamburger, T., Jurkat, T., Minikin, A., Petzold, A., Rautenhaus, M., Schlager, H., Schumann, U., Voigt, C., Spichtinger, P., Gayet, J., Gourbeyre, C., and Krämer, M.: Thin and subvisible cirrus and contrails in a subsaturated environment, Atmos. Chem. Phys, 11, 5853–5865, 2011.

Lamb, D. and Verlinde, J.: Physics and Chemistry of Clouds, Cambridge University Press, http://dx.doi.org/10.1017/CBO9780511976377, 2011.

Lawson, R. P., Pilson, B., Baker, B., Mo, Q., Jensen, E., Pfister, L., and Bui, P.: Aircraft measurements of microphysical properties of subvisible cirrus in the tropical tropopause layer, Atmospheric Chemistry and Physics, 8, 1609–1620, doi:10.5194/acp-8-1609-2008, http://www.atmos-chem-phys.net/8/1609/2008/, 2008.

McDonald, J.: Use of the electrostatic analogy in studies of ice crystal growth, Zeitschrift für angewandte Mathematik und Physik, 14, 610–620, doi:10.1007/BF01601268, http://dx.doi.org/10.1007/BF01601268, 1963.

Murphy, D. and Koop, T.: Review of the vapour pressures of ice and supercooled water for atmospheric applications, Quarterly Journal of the Royal Meteorological Society, 131, 1539–1565, 2005.

Pruppacher, H. R. and Klett, J. D.: Microphysics of clouds and precipitation, Kluwer Acad. Pub., Dordrecht, 1997.

Ramkrishna, D.: Population Balances, Academic Press, 2000.

Ren, C. and Mackenzie, A. R.: Cirrus parametrization and the role of ice nuclei, Quarterly Journal of the Royal Meteorological Society, 131, 1585–1605, doi:10.1256/qj.04.126, http://dx.doi.org/10.1256/qj.04.126, 2005.

Sassen, K. and Campbell, J. R.: A midlatitude cirrus cloud climatology from the Facility for Atmospheric Remote Sensing. Part I: Macrophysical and synoptic properties, Journal of the atmospheric sciences, 58, 481–496, 2001.

Sassen, K. and Dodd, G. C.: Haze particle nucleation simulations in cirrus clouds, and applications for numerical and lidar studies, Journal of the Atmospheric Sciences, 46, 1989.

Seifert, A. and Beheng, K.: A two-moment cloud microphysics parameterization for mixed-phase clouds. Part 1: Model description, Meteorology and atmospheric physics, 92, 45–66, 2006.

Nonlin. Processes Geophys. Discuss., doi:10.5194/npg-2015-78, 2016
Manuscript under review for journal Nonlin. Processes Geophys.
Published: 19 January 2016

Spichtinger, P. and Cziczo, D. J.: Impact of heterogeneous ice nuclei on homogeneous freezing events in cirrus clouds, Journal of Geophysical Research, 115, 2010.

Spichtinger, P. and Gierens, K. M.: Modelling of cirrus clouds–Part 1a: Model description and validation, Atmospheric Chemistry and Physics, 9, 685–706, 2009.

Stephens, G. L.: The influence of radiative transfer on the mass and heat budgets of ice crystals falling in the atmosphere, Journal of the Atmospheric Sciences, 40, 1729–1739, 1983.

Stubenrauch, C. J., Cros, S., Guignard, A., and Lamquin, N.: A 6-year global cloud climatology from the Atmospheric InfraRed Sounder AIRS and a statistical analysis in synergy with CALIPSO and CloudSat, Atmospheric Chemistry and Physics, 10, 7197–7214, doi:10.5194/acp-10-7197-2010, http://www.atmos-chem-phys.net/10/7197/2010/, 2010.

Verhulst, F.: Nonlinear differential equations and dynamical systems, Springer, 2 edn., 1996.

Wacker, U.: Structual stability in cloud physics using parameterized microphysics, Beiträge zur Physik der Atmosphäre, 65, 231–242, 1992.

Wacker, U.: Competition of Precipitation Particles in a Model with Parameterized Cloud Particles, J. Atmos. Sci., 52, 2577–2589, 1995.

Wacker, U.: Nonlinear effects in a conceptual multilayer cloud model, Nonlinear Processes in Geophysics, 13, 99–107, doi:10.5194/npg-13-99-2006, http://www.nonlin-processes-geophys.net/13/99/2006/, 2006.

Wang, P.-H., Minnis, P., McCormick, M. P., Kent, G. S., and Skeens, K. M.: A 6-year climatology of cloud occurrence frequency from Stratospheric Aerosol and Gas Experiment II observations (1985–1990), Journal of Geophysical Research, 101, 29 407–29 429, 1996.

Nonlin. Processes Geophys. Discuss., doi:10.5194/npg-2015-78, 2016
Manuscript under review for journal Nonlin. Processes Geophys.
Published: 19 January 2016

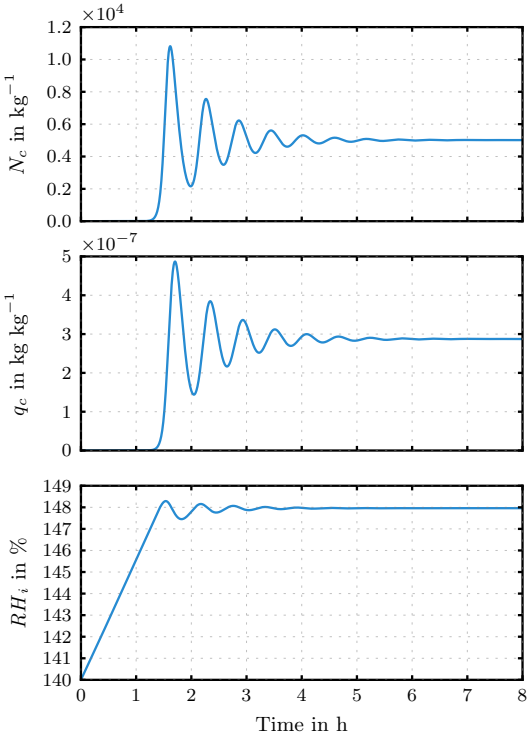

Figure 1. Here, a scenario in state 1 (damping) is shown at $w = 0.01\,\mathrm{ms}^{-1}$ and $T = 220\,\mathrm{K}$. The continuous nucleation as well as similar time scales of nucleation, growth and sedimentation lead to a damped oscillation with an equilibrium state for $t > 7$ h. In the phase space, the attractor property is visible (see figure 3).

Nonlin. Processes Geophys. Discuss., doi:10.5194/npg-2015-78, 2016
Manuscript under review for journal Nonlin. Processes Geophys.
Published: 19 January 2016

Nonlinear Processes in Geophysics
Discussions
Open Access
EGU

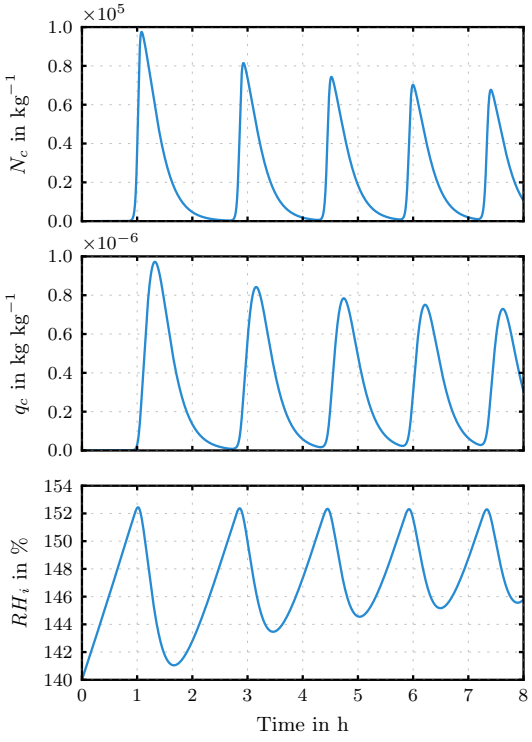

Figure 2. Here, a scenario in state 2 (limit cycle) is shown at $w = 0.02\,\mathrm{ms}^{-1}$ and $T = 210\,\mathrm{K}$. Nucleation events occur as pulses, thus an undamped oscillation evolves, which describes a limit cycle in the phase space (see figure 4).)

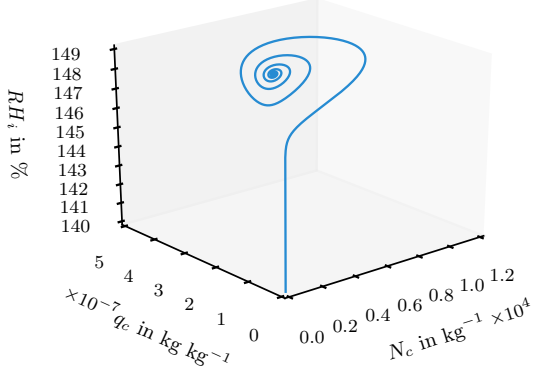

Figure 3. Positive attractor for state 1 at $T = 220\,\mathrm{K}$, $w = 0.01\,\mathrm{ms}^{-1}$: orbit in the phase space approaching the equilibrium point.

Nonlin. Processes Geophys. Discuss., doi:10.5194/npg-2015-78, 2016
Manuscript under review for journal Nonlin. Processes Geophys.
Published: 19 January 2016

Nonlinear Processes in Geophysics
Discussions
Open Access
EGU

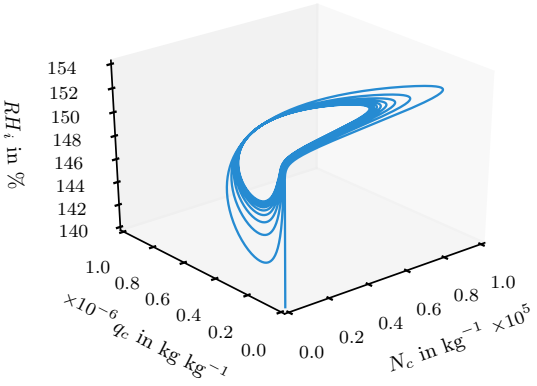

Figure 4. Limit cycle for state 2: orbit in the phase space at $T = 210\,\mathrm{K}$, $w = 0.02\,\mathrm{ms}^{-1}$

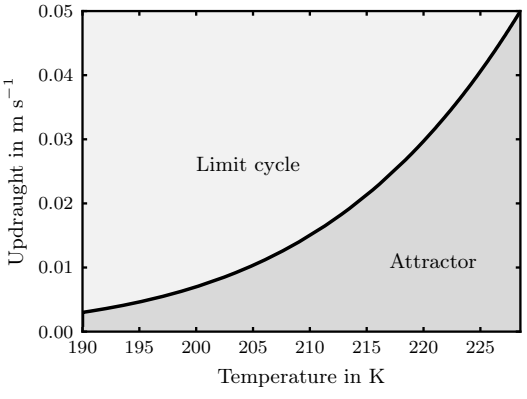

Figure 5. Bifurcation diagram for “positive attractor" (state 1) and “limit cycle" (state 2) regimes in the w-T-space. The thick line indicates the location of the Hopf bifurcation.

Nonlin. Processes Geophys. Discuss., doi:10.5194/npg-2015-78, 2016
Manuscript under review for journal Nonlin. Processes Geophys.
Published: 19 January 2016

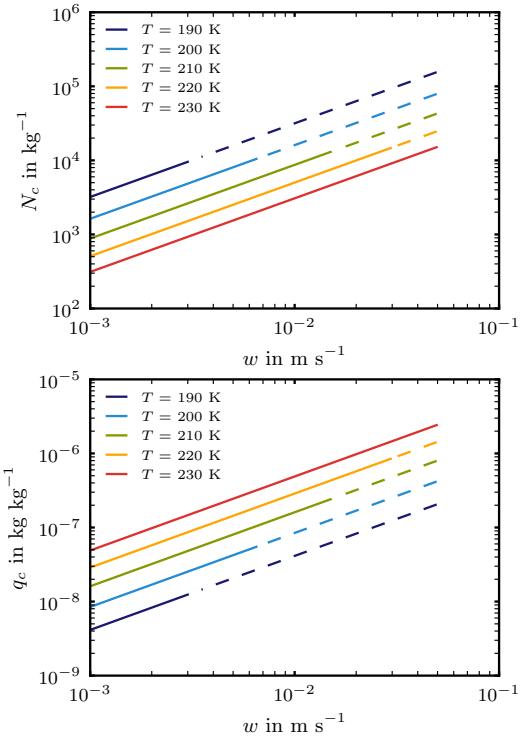

Figure 6. Ice particle number concentration N_c (upper panel) and ice particle mass concentration q_c (lower panel) at the critical point as a function of vertical velocity for different temperatures. Solid lines are for parameter combinations (w, T) in the attractor regime (state 1), dashed lines are for the limit cycle regime (state 2).

Nonlin. Processes Geophys. Discuss., doi:10.5194/npg-2015-78, 2016
Manuscript under review for journal Nonlin. Processes Geophys.
Published: 19 January 2016

Nonlinear Processes in Geophysics
Discussions
Open Access
EGU

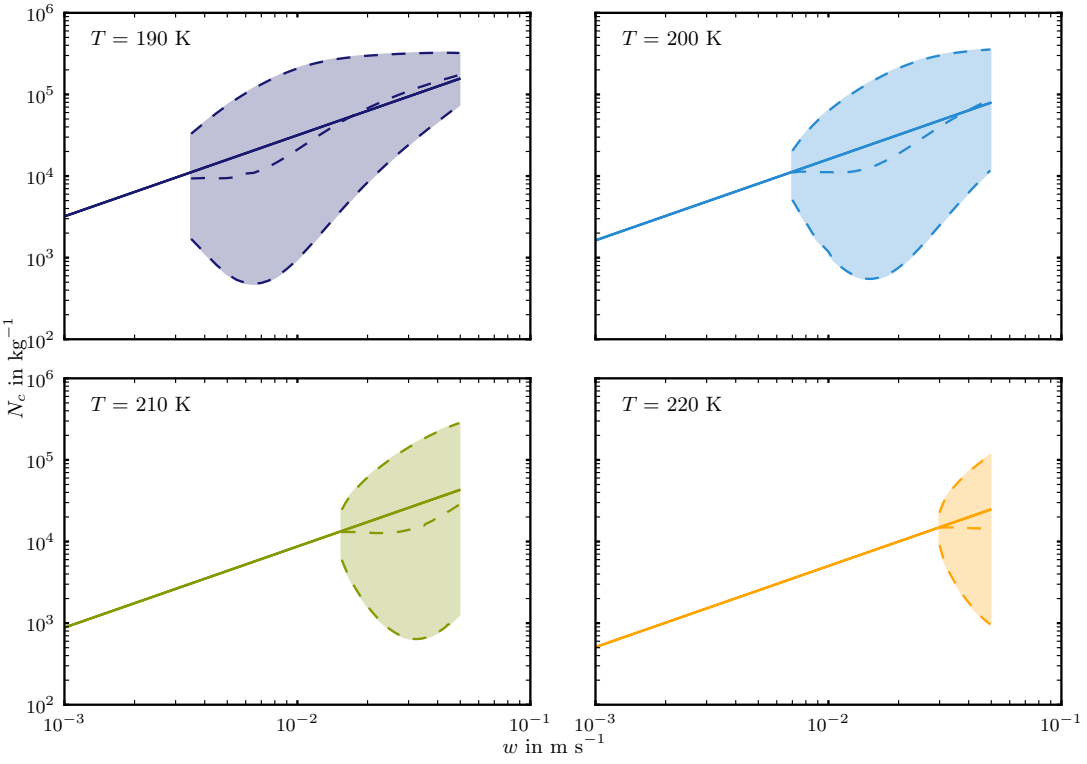

Figure 7. Ice crystal number concentrations for different temperature scenarios ($T = 190, 200, 210, 220\,\mathrm{K}$). The solid line represents values at the critical point $\boldsymbol{x}_0$. For the limit cycle regime the range of ice crystal number concentrations is indicated by the shaded area bounded by minimum and maximum values for the updraught range $0.001 \leq w \leq 0.05\,\mathrm{ms}^{-1}$; the median is indicated by the dashed line.

Nonlin. Processes Geophys. Discuss., doi:10.5194/npg-2015-78, 2016
Manuscript under review for journal Nonlin. Processes Geophys.
Published: 19 January 2016

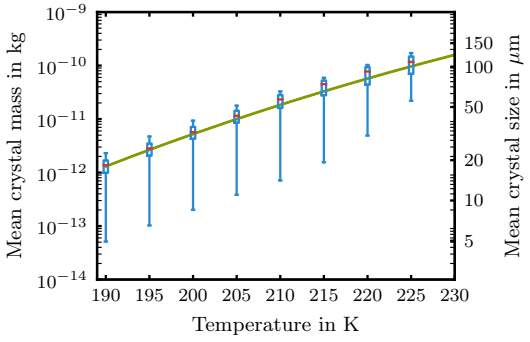

Figure 8. Mean ice crystal mass $\overline{m}$ as a function of temperature. For the critical point $\boldsymbol{x}_0$, values of $\overline{m}$ depends only slightly on the vertical velocity, the curve covers the area that corresponds to vertical velocities $0.001\,\mathrm{ms}^{-1} \leq w \leq 0.05\,\mathrm{ms}^{-1}$. Additionally, box and whiskers plots indicate median, 25%, 75% percentiles, and minimum/maximum values, respectively, for the limit cycle regime.

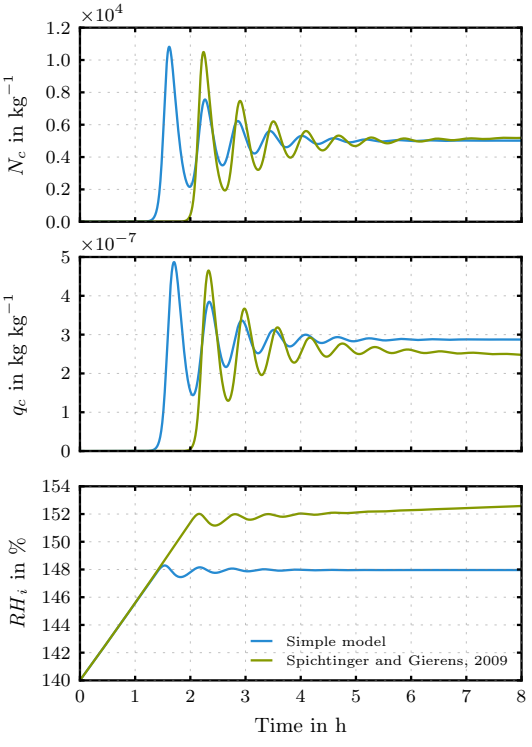

Figure 9. Attractor case (state 1): Comparison between simple box model and the complex model by Spichtinger and Gierens (2009). $w = 0.01\mathrm{ms}^{-1}$, temperature in the simple model and start temperature of the complex model is $T = 220\,\mathrm{K}$.

Nonlin. Processes Geophys. Discuss., doi:10.5194/npg-2015-78, 2016
Manuscript under review for journal Nonlin. Processes Geophys.
Published: 19 January 2016

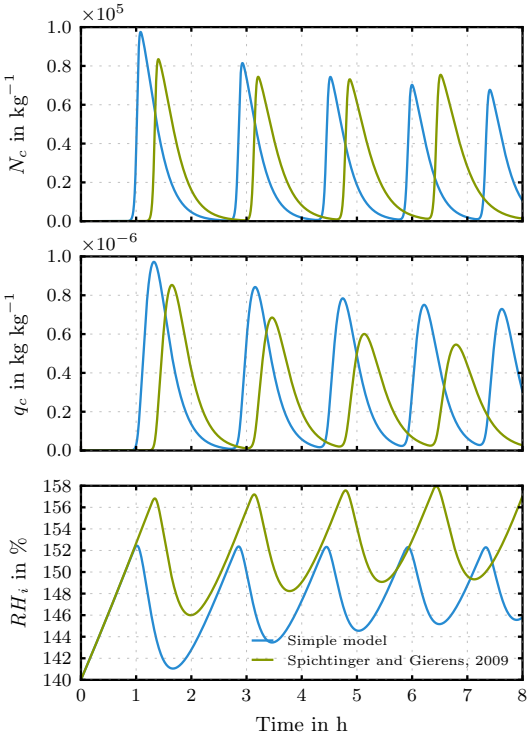

Figure 10. Limit cycle case (state 2): Comparison between simple box model and the complex model by Spichtinger and Gierens (2009). $w = 0.02\,\mathrm{ms}^{-1}$, temperature in the simple model and start temperature of the complex model is $T = 210\,\mathrm{K}$.

Nonlin. Processes Geophys. Discuss., doi:10.5194/npg-2015-78, 2016
Manuscript under review for journal Nonlin. Processes Geophys.
Published: 19 January 2016

Nonlinear Processes in Geophysics
Discussions
Open Access
EGU

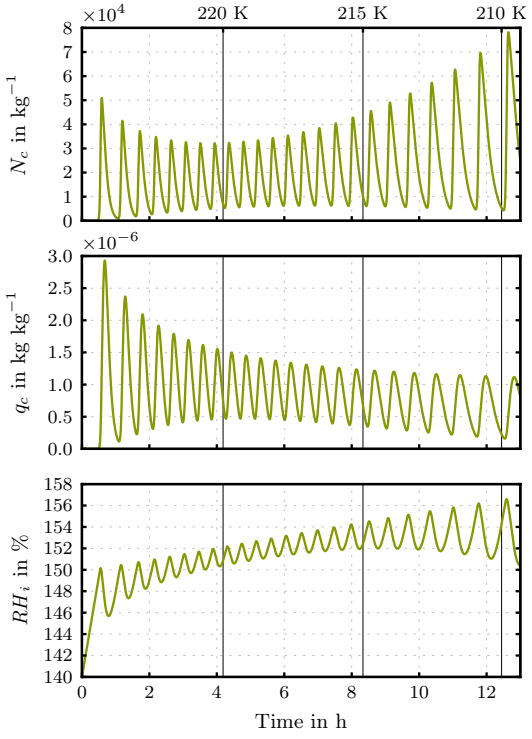

Figure 11. Transition between attractor regime (state 1) and limit cycle regime (state 2): Simulation with the complex model by Spichtinger and Gierens (2009) for $w = 0.035\mathrm{ms}^{-1}$ and start temperature: $T = 225\,\mathrm{K}$. During the first two hours of simulations, the attractor characteristics can be clearly seen. After reaching temperatures of about $T \sim 220\,\mathrm{K}$, the regime changes from state 1 (attractor) to state 2 (limit cycle), see also phase diagram in fig. 5. after this transition, the amplitudes of number concentrations and relative humidity w.r.t. ice increase and at the end of the simulation also a shift in the oscillation period can be seen due to temperature change.